INT. J. REMOTE SENSING, 20 NOVEMBER, 2003,
VOL. 24, NO. 22, 4543–4558

Taylor & Francis
Taylor & Francis Group

Correcting the orbit drift effect on AVHRR land surface skin temperature measurements

MENGLIN JIN

Department of Meteorology, University of Maryland, College Park, MD 20742, USA; e-mail: mjin@atmos.umd.edu

and R. E. TREADON

Environmental Modeling Center, National Centers for Environmental Prediction, Camp Springs, MD 20746, USA

(*Received 20 March 2002; in final form 13 November 2002*)

Abstract. The orbital drift of the National Oceanic and Atmospheric Administration (NOAA)-7, -9, -11, -14 series of satellites results in a significant cooling effect on their afternoon path Advanced Very High Resolution Radiometer (AVHRR) land surface skin temperature (T_s) measurements. This effect mixes with the signal of true variations in the climate system, and thus prevents T_s from being directly used in climate change and global warming studies. This paper applies a physically based 'typical pattern technique' to remove the orbit drift effect from T_s. The technique utilizes a lookup table of representative land skin temperature diurnal cycles derived from the National Center for Atmospheric Research (NCAR) Climate Community Model (CCM3) coupled with the land surface model, Biosphere–Atmosphere Transfer Scheme (BATS). The generated typical patterns of T_s diurnal cycle are functions of vegetation type, season and latitude, and are combined with satellite observations to remove the cooling effect. Applying this methodology to eighteen years of AVHRR (1981–1998) T_s observations yields an improved skin temperature dataset. Analysis of the drift-corrected skin temperature illustrates a warming trend at the surface over the past two decades, a result which agrees well with the observed surface air temperature trend. A discussion of uncertainties in this technique is also presented.

1. Introduction

A long-term, temporally consistent land surface skin temperature (T_s, hereafter, referred to as skin temperature) dataset is highly desirable for global climate studies (Jin and Dickinson 2002). National Oceanic and Atmospheric Administration (NOAA)-series Advanced Very High Resolution Radiometer (AVHRR) data have now been collected for more than twenty years. AVHRR skin temperature measurements, though attractive, cannot be directly used in climate change studies because of the orbit drift in the NOAA satellites (particularly, NOAA-7, -9, -11, and 14) over the course of these satellites' lifetime (Price 1991, Hurrell and

International Journal of Remote Sensing
ISSN 0143-1161 print/ISSN 1366-5901 online © 2003 Taylor & Francis Ltd
http://www.tandf.co.uk/journals
DOI: 10.1080/0143116031000095943

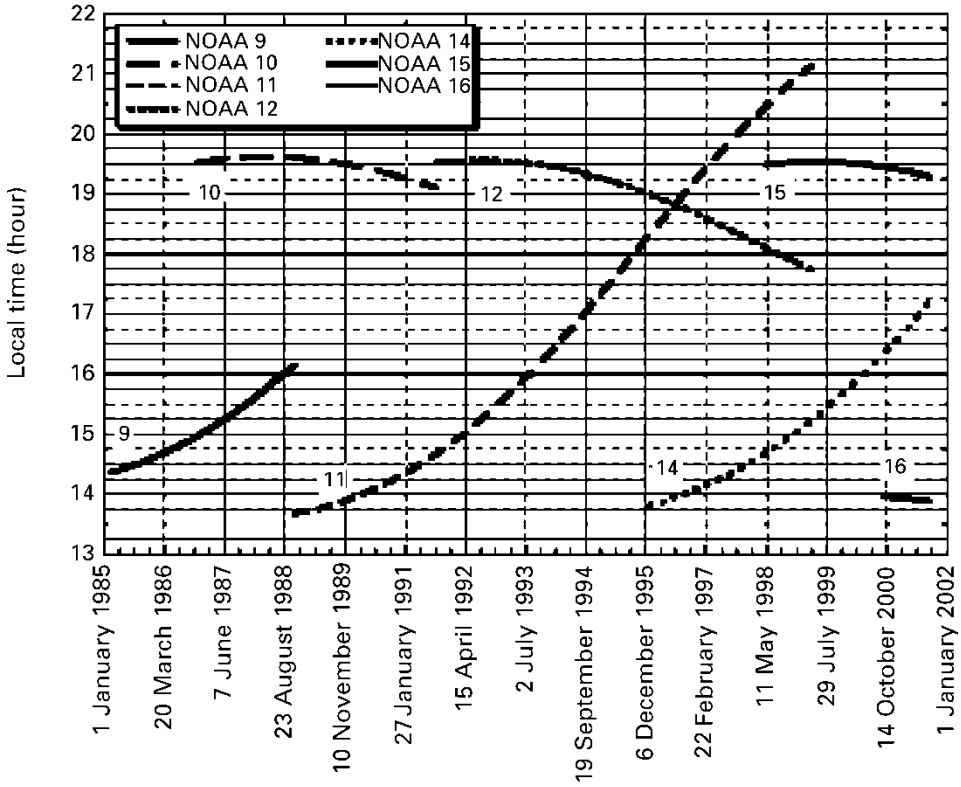

Figure 1. Schematic diagram of the equatorial crossing time for NOAA-9, -10, -11, -12, -14, -15 and -16. The y direction is local equatorial crossing time, and the x direction is time of year. NOAA-7 is not shown here but has similar orbital drift as the afternoon satellites NOAA-9, -11, -14. (Source, H. T. Lee, Department of Meteorology, University of Maryland.)

Trenberth 1998, Gutman 1999, J. Susskind, 2001, personal communication). Figure 1 schematically illustrates the change in the northbound equatorial crossing time due to orbit drift. For example, NOAA-11 initially observed the surface around 13:30 local time (LT) in 1989 but, by the end of 1994, its overpass time had shifted to 17:00LT. This drift is attributed to the selection of a satellite orbit designed to avoid direct sunshine on the instruments (Price 1991). The orbital drift leads to the measurements of surface skin temperature being taken at different local times during the satellites' lifetime, thereby introducing a temporal inconsistency in the T_s data. Consequently, such satellite drift results in a cooling trend in the satellite measured T_s. Figure 2 plots the global mean T_s measured using these satellites from 1981–1998, over land only. The data used to produce this figure came from the NOAA/National Aeronautic & Space Administration (NASA) Pathfinder AVHRR Land Surface Data Sets (PAL) (Agbu and James 1994). This dataset excludes Greenland and Antarctic snow-covered areas. These observations were made only under clear skies and thus some regions and seasons may be poorly sampled due to the contamination of clouds. Due to the orbit drift, a cooling trend over time is evident when looking at the dataset as a whole. Discontinuities

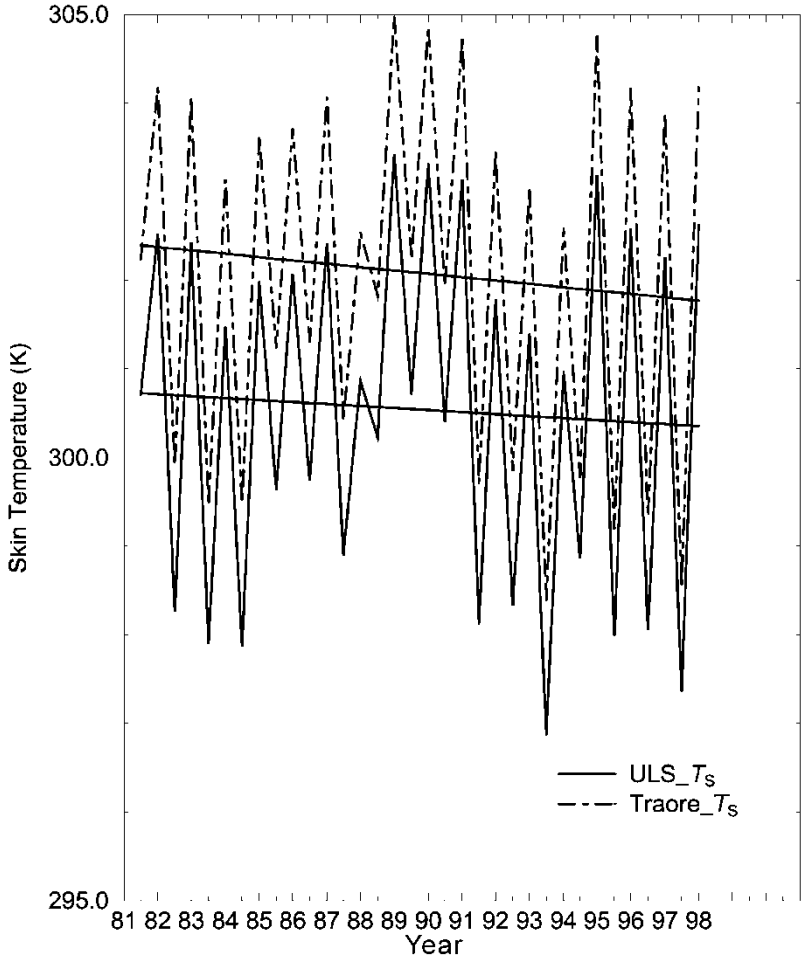

Figure 2. Annual global mean of AVHRR skin temperature. Annual mean is defined as the arithmetic average between January and July. T_s is calculated from two split-window equations: 'ULS-Tskin' is the Ulivieri algorithm (Ulivieri *et al.* 1994); and 'Traore-Tskin' is based on Traore *et al.* (1997). The straight lines are linear regressions for both T_s time series. The negative slopes of the straight lines indicate decreases of T_s from 1981 to 1998. The two T_s series demonstrate that while different split-window algorithms can produce different skin temperatures, the cooling effect caused by the orbit drift is similar in both series.

associated with the transition from one satellite to the next are also evident. For example, there is a 3–5°C difference between July 1988 and July 1989 when the observing satellite switched from NOAA-9 to -11. This difference is much larger than the expected interannual temperature variability, which is about 1–2°C at high latitude of Northern Hemisphere and 0.5–1°C at the low latitudes (Trenberth *et al.* 2001). To avoid mis-interpreting signals due to orbit drift and satellite changes, corrections must be applied to remove or, at least, reduce, these effects from the AVHRR T_s data. This paper introduces a practical, physically sound methodology to achieve this purpose.

Since the orbit drift effect was first reported (Price 1991), several methodologies

have been independently developed to correct for its effects on skin temperature (Gutman 1999, Jin and Dickinson 1999, Los *et al*. 2000). Some of these approaches used AVHRR-derived Normalized Difference Vegetation Index (NDVI) measurements to correct the temperature. For example, Gutman (1999) corrected the orbital drift on skin temperature by dividing the global land areas into different NDVI-based classes and then regressing the satellite solar zenith angle against the NDVI for each class. When applied to the PAL dataset, Gutman's method shows encouraging results in correcting the surface temperature cooling trend due to orbit drift. The advantage of this method is its simplicity, but it suffers from limitations in the determination of vegetation classes or unrepresentative samples used in computing the regression coefficients as trade off. Other correction techniques utilize additional satellite measurements or *in situ* data to correct the AVHRR-based skin temperature (Reynolds 1988). This approach is similar to the methodology used in data assimilation. While plausible in theory, specification of error characteristics and the presence of bias make it difficult in practice. In addition, in order to use other satellite data, a great deal of effort is required to ensure that the calibrations between different platforms are consistent. Furthermore, the use of *in situ* measurements is even more problematic, since *in situ* measurements sample the air temperature, not skin temperature. Deriving a physically realistic and robust mapping between these two temperatures remains a topic requiring further study (Jin *et al*. 1997).

Based on the first author's previous research addressing climate modelling and satellite skin temperature (Jin and Dickinson 1999), this paper describes a 'typical pattern technique' to correct AVHRR skin temperature observations. The technique is applied to 18 years (1981–1998) of AVHRR skin temperature data to convert temperatures measured at different local times to 14:00LT. Here, for simplicity, we focus only on January and July to conduct orbit-drift correction. Nevertheless, the technique could be easily expanded to other months. The annual mean is calculated as an average of January and July because these two months generally represent the maximum and minimum temperatures in the annual cycle and their average is adequate to capture the major features of the annual mean (J. Shuttleworth 1993, personal communication). The resulting corrected dataset provides a temporally consistent record which may be used to study global surface temperature variations over the past two decades.

The paper contains four more sections. Section 2 introduces the 'typical pattern technique' and describes the physical principles behind it. Section 3 briefly outlines the datasets, as well as the global climate model used in this research. Section 4 discusses the results and presents a brief analysis of uncertainties in the technique. Finally, more discussions and conclusions are given in section 5.

2. Methodology

The 'typical pattern technique' is described in detail by Jin and Dickinson (1999). The skin temperature diurnal cycle ($T_s(t)$, $t=1$ to 24) is decomposed into three parts: a climate mean diurnal cycle ($\bar{T}_s(t)$), instantaneous variations (T_s'), and noise $N(t)$:

$$T_s(t) = \bar{T}_s(t) + T_s'(t) + N(t), \tag{1}$$

with t ranging from 1 to 24. The climatological mean $\bar{T}_s(t)$ ($t=1$ to 24) represents

the typical diurnal cycle pattern. The noise term represents small-scale fluctuations or random measurement error. T'_s is the instantaneous disturbance from mean condition. The disturbance can be largely explained as the response of the atmospheric surface layer to short time-scale atmospheric forcing. Taking $N(t)$ to be negligible with respect to the typical pattern which represents most of the T_s diurnal cycle, the skin temperature diurnal cycle can be described as a combination of the typical pattern and instantaneous variations $\bar{T}_s(t)+T'_s(t)$, $t=1$ to 24.

The underlying physical basis for this decomposition is as follows. The diurnal cycle of surface temperature is dominated by the absorbed surface insolation. This forcing evolves over longer time-scales, i.e. climatology. However, the actual skin temperature also depends on the instantaneous state of the atmosphere and surface properties, such as wind and soil moisture. The first term in equation (1) corresponds to the typical diurnal cycle of T_s, which is a function of season, latitude and surface type (Jin and Dickinson 1999, 2000, Jin 2000), while the latter can be related to the instantaneous satellite observation of T_s. The typical patterns of the T_s diurnal cycle used in this research are taken from a global climate model (GCM), as described by Jin and Dickinson (1999). They analysed hourly output from long-term global simulations using the National Center for Atmospheric Research (NCAR) Climate Community Model (CCM3) coupled with the Biosphere–Atmosphere Transfer Scheme (BATS) land surface model. Look-up tables for typical patterns of the T_s diurnal cycle are obtained for all land covers, seasons and latitudes (see figure 4). If the corrected AVHRR T_s data are to be of value, the model used to build the T_s database must have a reasonable T_s climatology. The CCM3/BATS model is chosen to derive the look-up table because this GCM package generates a realistic skin temperature climatology (Jin *et al.* 1997). Further tests against Geostationary Operational Environmental Satellite (GOES) diurnal skin temperature measurements and field experiments (*in situ* observations) demonstrate that the typical patterns derived from this model describe physically acceptable diurnal cycles for T_s (Jin and Dickinson 1999).

Figure 3 shows some examples of the typical patterns of skin temperature for various conditions. Figure 3(*a*) illustrates the latitude dependence of typical patterns for vegetation type 3, i.e. evergreen needleleaf tree, at 45° N and 15° N. Vegetation types used here follow what are used in BATS, as listed in table 1. Figure 3(*b*) shows the seasonal dependence of typical patterns, representing the diurnal variations of skin temperature for evergreen needleleaf tree in January, April, July and October. Figure 3(*c*) shows the land cover dependence for three vegetation types (evergreen needle-leaf tree (veg3), vegetation type Tundra (veg9) and Bog or Marsh (veg13). The typical patterns are normalized using the equation:

$$\hat{T}_s(t)=(T_s(t)-T_{\min})/(T_{\max}-T_{\min}) \tag{2}$$

where $T_{\max}$ and $T_{\min}$ are the maximum and minimum temperatures of that typical pattern. This normalization is used to facilitate easy comparison between typical diurnal variations.

The look-up tables of diurnal cycle for skin temperature are given by Jin and Dickinson (1999) for each season. Figure 4 shows a look-up table for winter. Since typical patterns of the T_s diurnal cycle vary with latitude, land cover and season, the columns of figure 4 represent the total 18 vegetation types as defined in BATS (Dickinson *et al.* 1993; also see table 1). Latitude varies along the ordinate, and

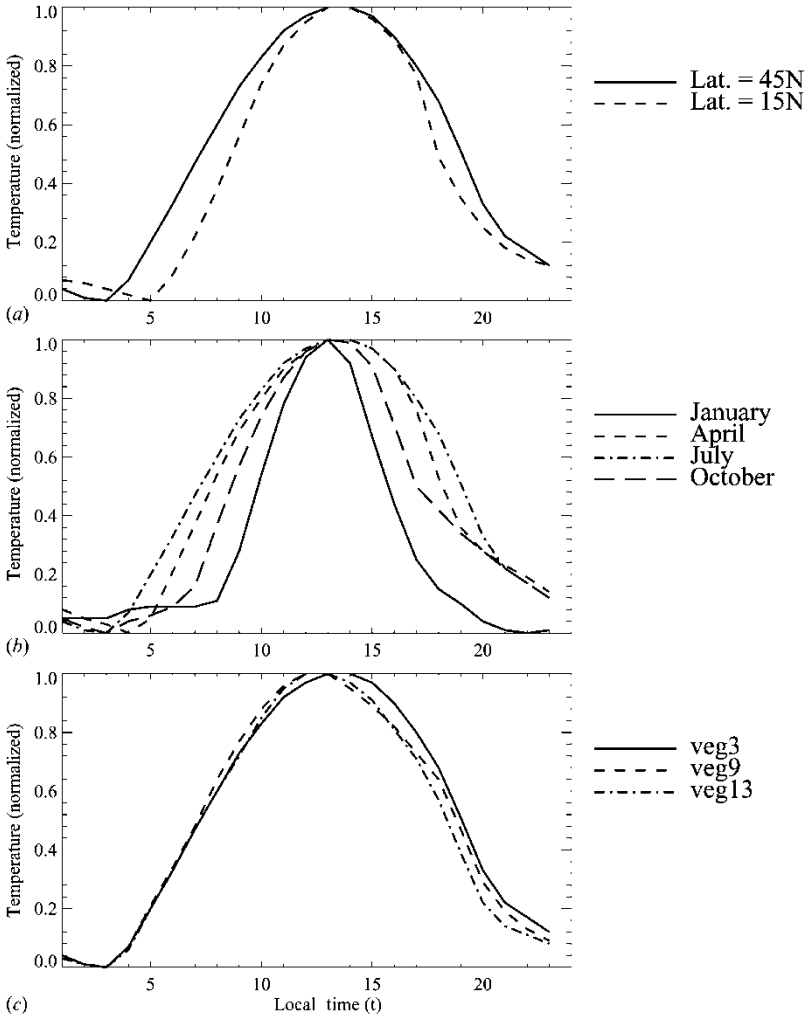

Figure 3. Examples of the typical patterns for T_s diurnal cycle: (*a*) shows the dependence of the typical pattern on latitude, for vegetation type 3 (evergreen needleleaf tree) in July; (*b*) shows the typical patterns of evergreen needleleaf tree for January, April, July and October; the latitude is 45° N; (*c*) shows the typical patterns for different vegetation types in July at 45° N. Veg3, veg9 and veg13 are vegetation types 3, 9 and 13, respectively (table 1).

local time for each column varies along the abscisa. For each 5° latitude band, we derived typical patterns for each vegetation/land cover type existing in that band. After normalization, the value of a typical pattern ranges from 0–1 as shown by the colour bar. Obviously, the differences between the typical patterns are significant which once again suggests that skin temperature diurnal cycle varies closely with surface properties and atmosphere conditions.

The look-up table is used to correct the orbital drift effect on the surface temperature and, consequently, to derive the temperature at a consistent time over the lifetime of each NOAA afternoon satellite. Figure 5 shows the three steps of this

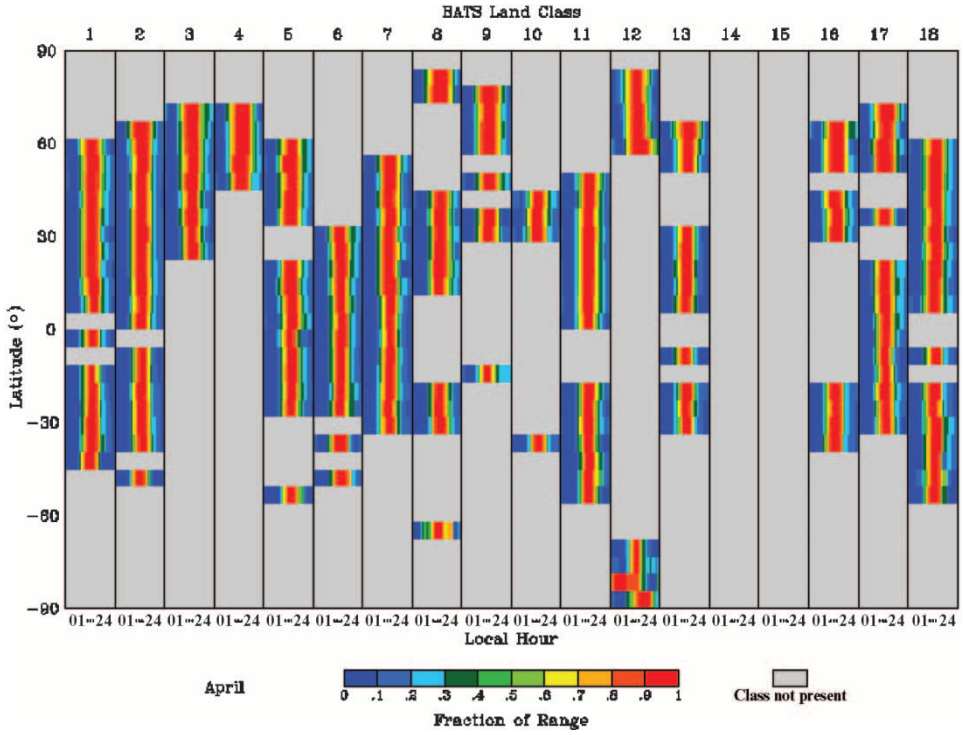

Figure 4. Look-up table for the normalized typical pattern of skin temperature diurnal cycle for CCM3/BATS, winter season only. The *x*-axis has 18 columns corresponding to the 18 surface types of BATS. The label of each column is 01 to 24, representing the hour of the day. The position of each colour bar in the column gives the normalized diurnal cycle for the vegetation at that latitude, and the value can be inferred from the colour bar at the bottom of the figure.

Table 1. Vegetation/land cover types.

Vegetation type	
1	Crop/mixed farming
2	Short grass
3	Evergreen needleleaf tree
4	Deciduous needleleaf tree
5	Deciduous broadleaf tree
6	Evergreen broadleaf tree
7	Tall grass
8	Desert
9	Tundra
10	Irrigated crop
11	Semi-desert
12	Ice cap/glacier
13	Bog or marsh
16	Evergreen shrub
17	Deciduous shrub
18	Mixed woodland

Taken from BATS (Dickinson *et al.* 1993).

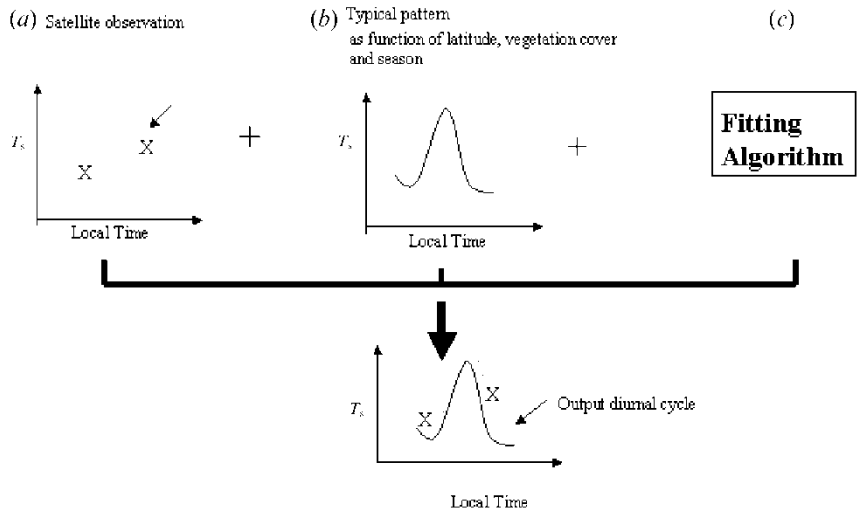

Figure 5. Schematic diagram of the 'typical pattern technique'. There are four components of this technique (*a*) is the satellite twice-per-day skin temperature observations; 'X' represents satellite T_s observation at one given location; (*b*) is an example of the corresponding typical pattern of skin temperature diurnal cycle. The typical pattern is extracted from the look-up table as shown in figure 4, based on the season, location and land cover of the pixel. (*c*) is the fitting algorithm combining satellite measurements with the typical pattern to obtain a diurnal cycle of skin temperature. And, finally, output the orbital drift-corrected diurnal cycle.

technique. First, for a given pixel, obtain the satellite T_s observation and extract the corresponding typical pattern from the look-up table based on land cover/vegetation type, season and latitude. Second, fit the satellite measurement with the typical pattern to provide the diurnal cycle. Third, select the temperature at a consistent time to output, for example, 14:00LT, from which to build the drift-corrected T_s dataset.

3. Data sources

3.1. *AVHRR observations*

In this research, we have used the NOAA/NASA Pathfinder AVHRR Land Data Set developed and archived at NASA DAAC (Agbu and James 1994). Eighteen years (1981–1998) of monthly, 8 km, global data, including channel 1 (*ch*1) reflectance, channel 4 and channel 5 (*ch*4 and *ch*5) brightness temperatures, solar zenith angle and land mask are stored in this dataset. The land cover dataset is that which is used by the land use group at the University of Maryland (DeFries *et al.* 1998), with an original resolution of 1 km and was mapped to 8 km resolution for use in this work.

3.2. *GCM simulations*

Hourly output of skin temperatures covering one year of CCM3/BATS (Dickinson *et al.* 1993, Kiehl *et al.* 1996) simulation are used to estimate the monthly mean diurnal cycles. As mentioned previously, the BATS model used here has an extensive history of use and has been shown to be a robust and reliable land

surface model. Jin *et al.* (1997) compared BATS-simulated skin temperature with observations and proved good agreements between the two. The CCM3/BATS-derived look-up table for skin temperature diurnal cycle (Jin and Dickinson 1999) applies to different seasons, and includes the normalized diurnal cycle typical pattern for different land covers and latitudes. Importantly, the typical patterns used in this paper could also be derived from other observed or simulated skin temperatures, for example GOES or field experiments. To the extent that observational data and the model are free of systematic errors, observations and model simulations should yield essentially the same result. More details of GCM simulations and typical patterns can be found in Jin *et al.* (1997) and Jin and Dickinson (1999).

4. Results and error analyses

4.1. *Results*

Since the diurnal temperature cycle varies with land cover, the same magnitude satellite drift leads to various degrees of cooling over different surfaces. For example, a drift in July over the Northern Hemisphere middle latitude desert areas from a local time of 14:00 to 17:00 decreases the temperature by 5–10°C, while a cooling of only 1–2°C is found over a grassy area. Therefore, the orbit drift correction should be a function of land cover, season and latitude. We need to separately correct skin temperature time series for various land cover types.

Figure 6 depicts an example of the drift-corrected T_s and the applied correction for July 1988 over the globe. During this period, the satellite observed T_s at 16:00LT. Figure 6(*a*) is the skin temperature after orbit drift correction, and figure 6(*b*) is the correction term over the globe: the cooling due to orbit drift is clearly evident in figure 6(*b*). The positive values over figure 6(*b*) suggest that over the whole globe, skin temperatures generally increase after removing the orbital drift effect. The latitude dependence of correction is once again evident. While high latitudes tend to have a 1–2°C increase, the largest increases reach 5–10°C over the mid-latitude desert areas. Small increases are observed in tropical forest areas. Although the overall corrections are reasonable, fine straight lines are observed in figure 6(*b*) over certain areas (for example, middle northern Africa). This highlights the limitations in this correction technique due to the way in which the typical patterns are defined. Namely, as noted earlier, the typical pattern used by the technique represents an average over five degree latitude bands. Thus, neighbouring latitudes falling within different bands may have very different typical patterns, thereby causing an artificially abrupt change in temperature. Use of more smoothly distributed typical pattern or the ground data of T_s diurnal cycle would be expected to remove these artificial lines. Yet, we can see from figure 6(*a*) that the corrected skin temperature distribution appears reasonable, suggesting that the artificial lines noted in figure 6(*b*), while undesirable, do not cause a significant error on the corrected T_s values and, therefore, the corrected dataset may be still useful for further research applications. Indeed, a closer examination of this error indicates that the number of pixels involved in these artificial lines is very small compared to the global number of land pixels and thus their effect is minor when the global mean skin temperature is considered. Global mean is the scale conventional studied in global warming studies.

After removing the orbit drift cooling effect, the long-duration AVHRR skin

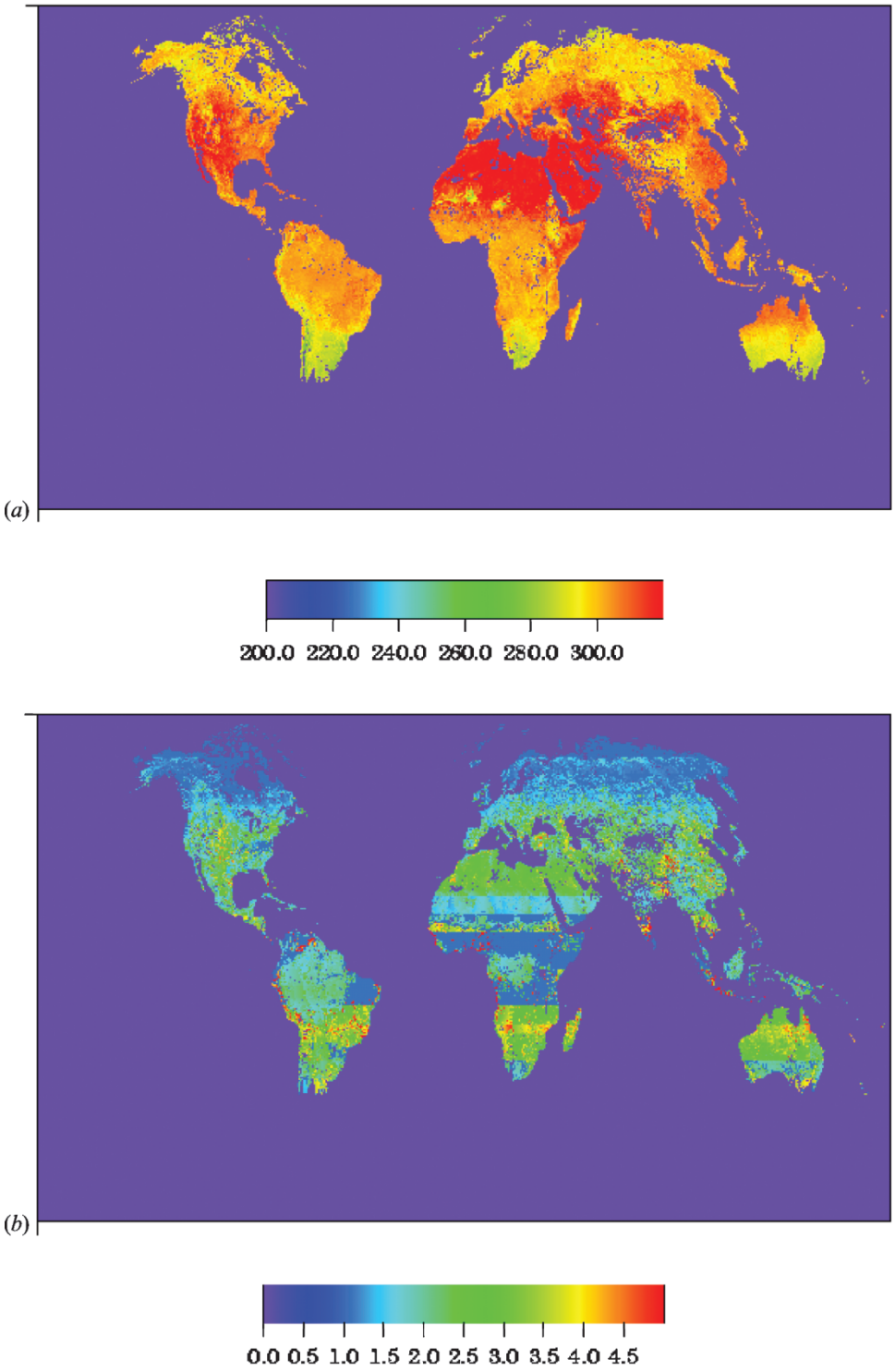

Figure 6. Global map of land surface skin temperature for orbit drift correction. The data are for July 1988. (*a*) Skin temperature after orbital drift correction. (*b*) Orbital drift corrected T_s minus the original satellite measured T_s. The pixels over the ocean are not considered.

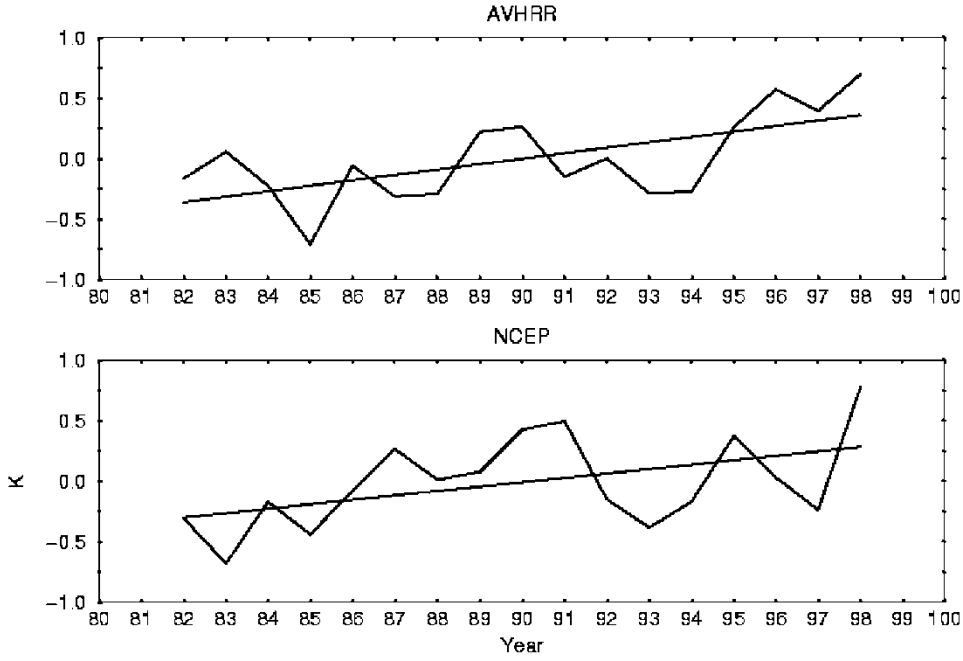

Figure 7. Anomalies of the annual global mean of orbital drift corrected skin temperature (land only). Here annual mean is calculated from the average of January and July. The x direction is year. The straight line is the linear regression. The upper panel is the orbital drift corrected AVHRR land surface skin temperature and the lower panel is the land surface skin temperature from the NCEP re-analysis.

temperature is valuable in studying global climate change. For example, Figure 7 shows the anomalies of global mean skin temperature for 1981–1998 based on data after the orbit-drift correction. The annual mean is an average of January and July. Comparing this figure with figure 2, the cooling effect of orbit drift on skin temperature disappears. Furthermore, the discontinuities at the satellite switch years (i.e. 1984–1985, 1988–1989, 1994–1995) are also reduced. The T_s trend over this period reveals an increase of about 0.4°C per decade. By comparison, figure 7(*b*) is the T_s trend computed from National Center for Environmental Prediction (NCEP) re-analysis data. An upward trend is also found in the NCEP data. The consistency of the T_s increase illustrated between the corrected AVHRR data and the NCEP re-analysis is encouraging, suggesting that the proposed orbit drift technique yields realistic results.

It is critical to validate the proposed approach from various temporal and spatial scales for future use in climate change studies. Figure 8 shows another validation for desert areas. Data are averaged for all desert pixels at 40–45° N in July. Evidently again, discontinuities at the satellite switch years (i.e. 1984–1985, 1988–1989, 1994–1995 as shown by the arrows) are corrected. For example, the minimum value is now observed in 1986 instead of at the end of the lifetime for NOAA-7. Discontinuities are also removed around the satellite switches in 1989 and in 1994. The overall increase of T_s in the late 1980s and the 1990s are consistent with both NOAA's TIROS Operational Vertical Sounder (TOVS) and surface

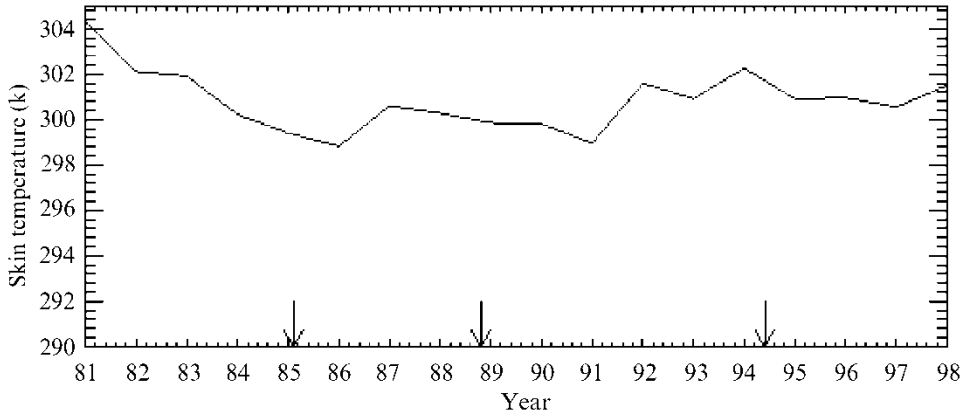

Figure 8. Orbit drift corrected interannual variation of AVHRR skin temperature for desert areas over 40–45° N. The satellite switch times are shown by the arrows.

temperature observations (J. Susskind, 2001, personal communication NRC 2000), suggesting the drift-corrected AVHRR data are now closer to the truth.

4.2. *Error analyses*

After applying the orbit drift correction, there remain other potential sources of error in T_s such as an incomplete drift correction, inaccurate skin temperature calibration, influence from volcanic eruptions and other sources such as limits in the split-window algorithm itself. With this in mind, T_s can be expressed as the following sum:

$$T_s = T_s^{true} + \delta T_s^{orbit} + \delta T_s^{calibration} + \delta T_s^{volcano} + \delta T_s^{others} \quad (3)$$

where T_s^{true} is the true, unknown, skin temperature. The other terms on the right side of equation (3) introduce errors into T_s. The 'typical pattern method' is designed to reduce errors due to orbit drift, the dominant uncertainty in temperature variation during the satellite lifetime (Price 1991). However, it may be difficult to accurately and completely remove this effect and, thus, δT_s^{orbit} remains as an error source, though at a reduced level. Another large uncertainty lies in $\delta T_s^{calibration}$, which includes all errors introduced during the skin temperature calibration procedure, such as incomplete atmospheric corrections, surface corrections, sensor degradation, change in solar zenith angle and unknown surface emissivity. Simply put, this term reflects inaccurate skin temperature measurement due to calibration or navigation algorithms. $\delta T_s^{volcano}$ is the uncertainty caused by volcanic eruptions, like that of Mt Pinatubo in June 1991. The overall effect of a volcano eruption is a cooling at the surface (McGregor and Gorman 1994, Long and Stowe 1994). This cooling ranges from 0.5–5°C. In fact, volcanic aerosol has two effects on skin temperature: one is the true cooling at the surface due to aerosol radiative forcing (Ramanathan *et al.* 2001); and the other is the contamination of the satellite retrieval due to an increased optical depth and the scattering of aerosol. The latter effect needs to be corrected in satellite skin temperature retrieval.

δT_s^{others} includes other error sources, for instance the split-window algorithm used in calculating T_s. Due to limitations in the split-window algorithm, the retrieved skin temperature of AVHRR has an accuracy of 1–3°C over land (Prata

et al. 1995, Wan 1996). Furthermore, calculating the pixel skin temperature in the presence of clouds also introduces uncertainties in T_s. For example, the AVHRR data in the NASA DAAC sometimes use the 2 m air temperature to replace the cloudy-pixel's skin temperature. This results in an inconsistency in the data due to physical and magnitude differences between satellite skin and surface screen air temperatures (Norman and Becker 1995).

Finally, the typical pattern look-up table derived from NCAR CCM3/BATS simulations can also be improved. Although the CCM3/BATS has been shown to simulate skin temperatures reasonably well (Jin *et al.* 1997), the model tends to describe the climatology rather than each day's skin temperature. Therefore, the statistically typical pattern may inaccurately model daily skin temperature variations. In addition, model performance depends on other surface variations such as albedo, emissivity, or parametrizations of small-scale physical processes, therefore, errors in these components would lead to errors in the skin temperature simulation. It is desirable to rebuild the typical pattern look-up table using more advanced, better resolution climate modelling systems, such as the NCAR Community Atmosphere Model coupled with the community land model (CAM2/CLM). The tables could also be constructed from more accurate observations of the diurnal cycle as these become available, such as from GOES or field experiments, for typical vegetation patterns and urban conditions.

5. Discussion and summary

As a summary, the orbit drift of the NOAA series satellites, among other factors, has a significant effect on the magnitude of the energy signal measured by the satellite sensors and, consequently, on the values of skin temperature. By combining GCM simulations with satellite observations, we have developed a look-up table of typical patterns for the skin temperature diurnal cycle to remove the drift effect. Testing this 'typical pattern technique' over an 18-year long AVHRR dataset shows that we can largely correct the cooling effect due to orbit drift and, thus, produce temporally consistent AVHRR skin temperature time series. There are, however, some comments.

1. The typical pattern look-up table approach proposed here shows encouraging results. The look-up table itself, nevertheless, can be improved by using more advanced climate–land surface models which can simulate more realistic land surface skin temperature diurnal cycle patterns. The look-up tables can also be derived from satellite observations such as GOES, assuming the retrievals have proven quality.
2. Since the typical patterns of diurnal cycle are currently model based, it is paramount that deficiencies in the model patterns be understood and well documented. Jin and Dickinson (1999) and Jin *et al.* (1997) have partially studied the use of model skin temperature diurnal cycle and compared it with First ISLSCP Field Experiment (FIFE), the Boreal Ecosystem–Atmosphere Study (BOREAS) and GOES observations. Further studies on this direction will be important and insightful.
3. The discrete, artificial gradients in the surface temperature corrections (figure 6(*b*)) warrant additional comment. The source of the gradient is unclear – it may result from the previously mentioned sampling method used to construct the typical patterns or it may come from an AVHRR data

discontinuity. The monthly AVHRR data were derived from ten-day composites using days when the maximum NDVI occurs. Therefore, the ten-day AVHRR skin temperature composites dataset may itself be discrete. The line evident in the correction term seems to be more related to the former. Nevertheless, the skin temperature field (figure 6(*a*)), namely the original AVHRR skin temperature after correction, does not reveal such discrete features. Furthermore, these features form a very small portion of the dataset and are removed when working with coarser resolutions, such as a half degree (not shown). This suggests that the dataset may still be useful in climate studies. We discuss this problem here with the expectation that it will be resolved in the near future. At the same time we want potential users to be aware of this problem.

4. It is important to keep in mind that in order to develop a long-term skin temperature dataset using our approach, or another similar typical pattern approach, the diurnal range of the typical pattern should not be fixed. In our approach, the typical patterns are normalized to 0–1. The normalized typical patterns are then converted into true diurnal cycle using twice-per-day skin temperature observations. Here, the diurnal range is determined from satellite day and night-time observations. If one uses our typical patterns but with their diurnal range not changed from the 1980s to the 1990s (as in Gleason *et al*. 2002, for example), and employs afternoon AVHRR data only to fit the absolute diurnal cycle, it may be appropriate for individual observations but precludes detection of any variation involving changes in the diurnal range. The global warming signal is characterized by much larger changes at night than during the day so fixing the diurnal range in developing a long-term data set loses the signal of global warming (Dai *et al*. 1996, Jin and Dickinson 2002). In addition, it may strongly bias inferences about regional patterns for similar reasons.

Acknowledgment

This research is funded by NASA EOSIDS program under contract ORA-99-OES04. We thank Mr Art Glean for providing us with AVHRR land cover data. Thanks also go to the editor and anonymous reviewers for their constructive comments.

References

AGBU, P. A., and JAMES, M. E., 1994, *The NOAA/NASA Pathfinder AVHRR Land Data Set Users Manual* (Greenbelt, MD: Goddard Distributed Active Archive Center, NASA, Goddard Space Flight Center).

DAI, A., TRENBERTH, K. E., and KARL, T. R., 1999, Effects of clouds, soil moisture, precipitation, and water vapor on diurnal temperature range. *Journal of Climate*, **12**, 2451–2473.

DEFRIES, R. S., HANSEN, M., TOWNSHEND, J. R. G., and SOHLBERG, R., 1998, Global land cover classifications at 8 km spatial resolution: the use of training data derived from Landsat imagery in decision tree classifiers. *International Journal of Remote Sensing*, **19**, 3141–33168.

DICKINSON, R. E., HENDERSON-SELLERS, A., and KENNEDY, P. J., 1993, *Biosphere–Atmosphere Transfer Scheme (BATS) Version 1E as Coupled to the NCAR*

Community Climate Model. NCAR Tech. Note, NCAR/TN-387+STR, pp. 72 National Center for Atmosphere Research, Boulder, CO.

GLEASON, A. C. R., PRINCE, S. D., GOETZ, S. J., and SMALL, J., 2002, Effects of orbital drift on land surface temperature measured by AVHRR thermal sensors. *Remote Sensing of Environment*, **79**, 147–165.

GUTMAN, G., 1999, On the use of land surface temperatures with the NOAA/AVHRR: removing the effect of satellite orbit drift. *International Journal of Remote Sensing*, **20**, 3407–3413.

HURRELL, J. W., and TRENBERTH, K. E., 1998, Difficulties in obtaining reliable temperature trends: reconciling the surface and satellite microwave sounding unit records. *Journal of Climate*, **11**, 945–967.

JIN, M., 2000, Interpolation of surface radiation temperature measured from polar orbiting satellites to a diurnal cycle. Part 2: Cloudy-pixel Treatment. *Journal of Geophysical Research*, **105**, 4061–4076.

JIN, M., and DICKINSON, R. E., 1999, Interpolation of surface radiative temperature measured from polar orbiting satellite to a diurnal cycle. Part 1: Without clouds. *Journal of Geophysical Research*, **104**, 2105–2116.

JIN, M., and DICKINSON, R. E., 2000, A generalized algorithm for retrieving cloudy sky skin temperature from satellite thermal infrared radiances. *Journal of Geophysical Research*, **105**, 27 037–27 047.

JIN, M., and DICKINSON, R. E., 2002, New observational evidence for global warming from satellite data set. *Geophysical Research Letters*, **29**, 10 1029/2001GL013833.

JIN, M., DICKINSON, R. E., and VOGELMANN, A. M., 1997, A comparison of CCM2/BATS skin temperature and surface–air temperature with satellite and surface observations. *Journal of Climate*, **10**, 1505–1524.

KIEHL, J. T., HACK, J. J., BONAN, G. B., BOVILLE, B. A., BRIEGLEB, B. P., WILLIAMSON, D. L., and RASCH, P. J., 1996, *Description of the NCAR Community Climate Model (CCM3). NCAR Technical Note*, NCAR/TN-420+STR (Boulder, CO: National Centre for Atmospheric Research).

LONG, C. S., and STOWE, L. L., 1994, Using the NOAA/AVHRR to study stratospheric aerosol optical thickness following the Mt. Pinatubo eruption. *Geophysical Research Letters*, **21**, 2215–2218.

LOS, S. O., COLLATZ, G. J., SELLERS, P. J., MALMSTROM, C. M., POLLACK, N. H., DEFRIES, R. S., BOUNOUA, L., PARRIS, M. T., TUCKER, C. J., and DAZLICH, D. A., 2000, A global 9-yr biophysical land surface data set from NOAA AVHRR data. *Journal of Hydrometeorology*, **1**, 183–199.

MCGREGOR, J., and GORMAN, A. J., 1994, Some consideration for using AVHRR data in climatological studies. 1. Orbital characteristics of NOAA Satellites. *International Journal of Remote Sensing*, **15**, 537–548.

NORMAN, J. M., and BECKER, F., 1995, Terminology in thermal infrared remote sensing of nature surfaces. *Agriculture and Forest Meteorology*, **77**, 153–166.

NRC, 2000, *National Research Council, Reconciling Observations of Global Temperature Change* (National Academy Press).

PRATA, A. J., CASELLES, V., COLLAND, C., SOBRINO, J. A., and OTTLE, C., 1995, Thermal remote sensing of land surface temperature from satellites: current status and future prospects. *Remote Sensing Reviews*, **12**, 175–224.

PRICE, J. C., 1991, Timing of NOAA afternoon passes. *International Journal of Remote Sensing*, **12**, 193–198.

RAMANATHAN, V., CRUTZEN, P. J., KIEHL, J. T., and ROSENFELD, D., 2001, Aerosol, climate, and the hydrological cycle. *Science*, **294**, 2119–2124.

REYNOLDS, R. W., 1988, A real-time global sea surface temperature analysis. *Journal of Climate*, **1**, 75–86.

TRAORE, P. C. S., ROYER, A., and GOITA, K., 1997, Land surface temperature time series derived from weekly AVHRR GVI composite data set: Potential and constraints for Northern Latitudes. *Canadian Journal of Remote Sensing*, **23**, 390–400.

TRENBERTH, K. E., STEPANIA, D. P., and HURRELL, J. W., 2001, Quality of reanalysis in the tropics. *Journal of Climate*, **14**, 1499–1510.

ULIVIERI, C., CASTRONUOVO, M. M., FRANCIONI, R., and CARDILLO, A., 1994, A

split-window algorithm for estimating land surface temperature from satellites. *Advances in Space Research*, **14**, 59–65.

WAN, Z., 1996, *MODIS Land-Surface Temperature Algorithm Theoretical Basis Document* (LST ATBD). NASA Contract NAS5-31370.